AIAA JOURNAL
Vol. 32, No. 8, August 1994

Onset of Vortex Breakdown Above a Pitching Delta Wing

Miguel R. Visbal*
Wright Laboratory, Wright-Patterson Air Force Base, Ohio 45433

Computational results are presented for transient vortex breakdown above a delta wing subject to a pitch-and-hold maneuver to high angle of attack. The flows are simulated by solving the full three-dimensional Navier-Stokes equations on a moving grid using the implicit Beam-Warming algorithm. An assessment of the effects of numerical resolution and favorable comparison with experimental data suggest the computational approach captures the basic dynamics of the onset and initial stages of transient breakdown. The pressure gradient along the vortex axis is found to play a dominant role in the initiation of breakdown. A description of the three-dimensional instantaneous structure of the flowfield is provided for the first time using critical-point theory. The reversed-flow region in the vortex core is associated with pairs of opposite spiral/saddle critical points. At its onset, the vortex breakdown is fairly axisymmetric; however, as it proceeds upstream and a stronger jump takes place along the axis, asymmetric effects become important and culminate in the formation of a bubble-type breakdown. This bubble structure is open and contains within itself a pair of stagnation points that are diametrically opposed and that rotate in the same sense as the upstream swirling flow. These critical points suggest the existence of azimuthal disturbances in the breakdown region. The bubble sectional topology is also found in agreement with recent experimental measurements.

Nomenclature

C	= wing chord
C_m	= pitching moment coefficient about midchord
C_p	= pressure coefficient, $2(p - p_\infty)/\rho U_\infty^2$
S^+, S^-	= attracting and repelling three-dimensional spiral/saddle critical points
t	= time
t^+	= nondimensional time, tU_∞/C
U'	= axial velocity component
U_∞	= freestream velocity
u, v, w	= velocity components in wing frame of reference
X_b	= chordwise location of vortex breakdown
X, Y, Z	= Cartesian coordinate system attached to the wing
X', Y', Z'	= coordinate system attached to wing apex and aligned with vortex axis
α	= angle of attack
Ω	= pitch rate, rad/s
Ω^+	= nondimensional pitch rate, $\Omega C/U_\infty$

Introduction

STUDY of the unsteady aerodynamics of delta wings at high angle of attack is motivated by current interest in enhanced aircraft maneuverability. Ashley et al.[1] have recently reviewed experimental work on delta wings pitching to high incidence. This work shows that, during transient high-angle-of-attack maneuvers, a lag in the onset of the leading-edge vortex breakdown occurs[2-4] as compared with a stationary wing. This lag is also accompanied by overshoots in the wing aerodynamic loads.[3,5] The initiation and unsteady behavior of vortex breakdown represents therefore one of the central issues in high-angle-of-attack aerodynamics. From a more general perspective, vortex breakdown is also observed in swirling flow devices, combustion chambers, trailing vortices, and tornadoes. Excellent reviews of experimental and theoretical work on vortex breakdown are given by Hall,[6] Leibovich,[7,8] and Escudier.[9]

The structure of vortex breakdown has been traditionally studied[10-12] using standard flow visualization techniques. Although of great value, these visualizations do not provide a precise definition of the complex three-dimensional unsteady structure of the flow. For instance, a clear distinction between the spiral and bubble forms of breakdown, based on the actual topology of the velocity or vorticity field, is not currently available. To overcome these limitations, recent experimental studies[13-18] have concentrated on detailed measurements of the velocity field. In addition, a few computational studies of three-dimensional vortex breakdown have been conducted (see, for instance, Refs. 19–21).

The present numerical study seeks to describe the unsteady flow structure above a pitching delta wing during the onset and initial stages of transient vortex breakdown. To achieve this goal, calculations are performed for a 75-deg sweep delta wing that is pitched at a constant rate to a high angle of attack. Conditions corresponding to the low-Reynolds-number experiments of Refs. 13 and 16 are selected for the purpose of comparison. The selection of a low Reynolds number (9.2×10^3 based on the wing chord) eliminates the uncertainties associated with turbulence modeling and diminishes grid resolution requirements. Nonetheless, as the results will show, this Reynolds number is high enough for nonaxisymmetric and unsteady features to be present, which are inherent to any realistic vortex breakdown flow. Furthermore, since the wing is pitched at a high rate, a well-defined axial pressure gradient is imposed on the leading-edge vortex. This dominant pressure gradient effect, which arises naturally from the external flow, makes the present configuration more attractive than that of an isolated vortex,[20,21] where breakdown is controlled by the specified (and somewhat artificial) boundary conditions.

The flows are simulated by solving the unsteady three-dimensional compressible Navier-Stokes equations on a moving grid using a time-accurate implicit solver that has been previously validated. In this study, only one half of the delta wing is considered, and the flow is assumed to be fully symmetric about the wing centerline. This is done to provide better numerical resolution of the breakdown region. The validity of this assumption may be judged a posteriori by the good comparison with the experiments. An assessment of the effects of grid resolution on the computed results is presented. Comparisons with experiments[13,16] are provided in terms of the instantaneous vortex breakdown location and flow structure. A characterization of the three-dimensional instantaneous struc-

Received April 13, 1993; revision received Dec. 21, 1993; accepted for publication Jan. 21, 1994.

*Aerospace Engineer, CFD Research Branch, Aeromechanics Division. Senior Member AIAA.

ture of the breakdown region is given for the first time using concepts from critical-point theory.[22] These computational results are also helpful in the interpretation of experimental velocity measurements usually obtained in selected planes through the flow.

Methodology

Governing Equations and Numerical Procedure

The governing equations are the full unsteady, three-dimensional compressible Navier-Stokes equations written in strong conservation law form.[23] Closure of this system of equations is provided by the perfect gas law, Sutherland's viscosity formula, and the assumption of a constant Prandtl number ($Pr = 0.72$). To deal with the case of external flow past a body in general motion, a time-dependent coordinate transformation is incorporated.

The governing equations are numerically solved employing the implicit approximate-factorization Beam-Warming algorithm.[24] The scheme is formulated using Euler implicit time-differencing and second-order finite difference approximations for all spatial derivatives. Fourth-order explicit and second-order implicit damping terms are added to control spurious numerical oscillations.[25] Newton subiterations[26,27] are also incorporated to reduce linearization and factorization errors, thereby improving the temporal accuracy and stability properties of the algorithm. A fully vectorized, time-accurate, three-dimensional Navier-Stokes solver has been developed using this scheme. The code has been validated for a variety of both steady and unsteady flows, including dynamic stall of a pitching airfoil, Taylor-vortex flow,[28] delta wings,[27,29] juncture flows,[30] and flow past a pitching forebody.[31]

Grid Structure and Boundary Conditions

The computational grid for the flat-plate delta wing is of the H-H type[27] and is obtained using simple algebraic techniques. Three different grids of sizes $98 \times 115 \times 102$ (grid 1), $141 \times 115 \times 118$ (grid 2), and $167 \times 115 \times 118$ (grid 3) in the ξ, η, and ζ directions, respectively, have been employed to assess resolution effects. The ξ, η, and ζ directions correspond to the streamwise, spanwise, and normal directions relative to the delta wing. For the finer grid, the minimum spacing normal to the wing is $\Delta Z/C = 0.0001$, the spacing along the wing leading edge varies from $\Delta Y/C = 5 \times 10^{-5}$ at the apex to 5×10^{-4} at the trailing edge, and the streamwise spacing on the wing is $\Delta X/C = 0.005$. It should be noted that the streamwise spacing was varied by a factor of 4 in the breakdown region to assess grid resolution effects. The far-field boundaries for all grids are located two chord lengths away from the delta wing. The effect of far-field boundary placement was investigated[32] for an 80-deg sweep delta wing at a 30-deg angle of attack and was found to be insignificant when the distance from the far-field boundary to the wing was increased from 1.5 to 3.0 chord lengths. The boundary conditions are implemented as described in Ref. 27. At the lower, upper, side, and upstream boundaries, characteristic conditions[33] are specified. On the downstream boundary, flow variables are extrapolated from the interior. Symmetry conditions are imposed along the midplane of the wing. On the wing surface, the following conditions are applied:

$$U = U_b$$

$$\frac{\partial T}{\partial \zeta} = 0$$

$$\frac{\partial p}{\partial \zeta} = \rho a_b \cdot \hat{n}$$

where U_b and a_b denote, respectively, the surface velocity and acceleration of the pitching wing given by the prescribed motion. For the present computations, a pitch-and-hold maneuver is considered in which the wing accelerates from rest to a constant pitch rate and then decelerates as it reaches its final angle of attack.

Critical-Point Theory

As noted earlier, one of the objectives of the present study is the description of the unsteady structure of vortex breakdown above the wing. For this purpose, the instantaneous velocity field within the leading-edge vortex is examined. The interpretation of instantaneous two-dimensional and three-dimensional streamline patterns is aided considerably by the use of critical-point theory or phase-space analysis.[22,34-37] At critical (or singular) points of the flow, the velocity is zero, and the streamline slope is indeterminate. Critical points are broadly divided into no-slip and free-slip critical points depending upon whether they are located on a no-slip boundary or within the fluid, respectively. For the present study, only the latter type will be considered in describing the vortex breakdown structure above the wing.

The classification of critical points and the elementary flow patterns in their vicinity are obtained by a linearized Taylor-series expansion of the velocity about the critical point.[22,36] A description of two-dimensional critical points can be found in Refs. 34 and 36. The general classification of three-dimensional critical points is given by Chong et al.[22] The concept of three-dimensional critical points has been used[35,36] in the analysis of flows predominantly when the critical points are located on no-slip surfaces or on symmetry planes and are therefore easily identifiable. In complex flows such as asymmetric vortex breakdown, free-slip critical points cannot be so easily located, and, in fact, a systematic topological description of this flow is not known to the author. In the present study, the only types of three-dimensional free-slip critical points encountered in the description of vortex breakdown are spiral/saddles (see Ref. 22). The topological analysis of the computed flowfields is accomplished using PLOT3D and FAST visualization software.[38]

Results

Calculations were performed for a 75-deg sweep delta wing at a freestream Mach number of 0.2 and a chord Reynolds number of 9.2×10^3. The wing was pitched at a nominal constant nondimensional pitch rate $\Omega^+ = \Omega C/U_\infty = 0.3$, from an initial angle of attack $\alpha_i = 25$ deg to a final angle $\alpha_f = 50$ deg (see Fig. 1). The pitch axis was located at the wing trailing edge. The previous conditions were selected to allow compari-

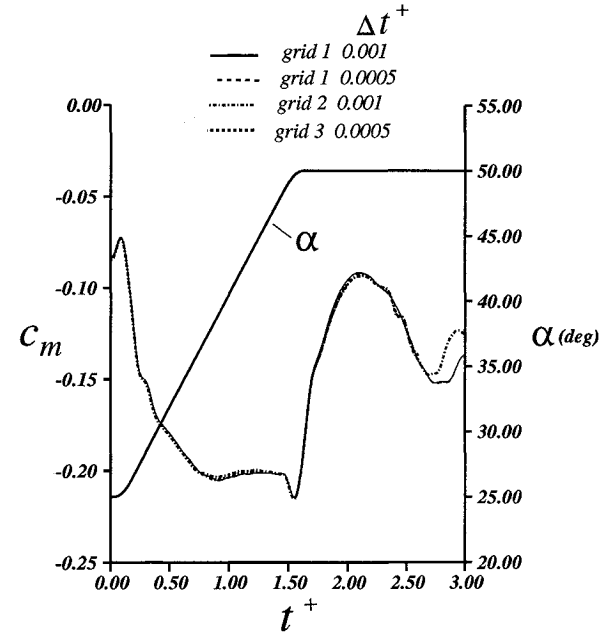

Fig. 1 Effect of numerical resolution on computed pitching moment coefficient.

son with the experiments of Magness, Robinson, and Rockwell[13] and Lin and Rockwell.[16]

Numerical Resolution Effects

Before proceeding to the discussion of the physical aspects of the flow, results from a limited assessment of the effects of numerical resolution on the computed solution are presented. The sensitivity of the computed flowfield to spatial resolution was investigated by employing the three grids previously described. The temporal accuracy was checked by computing the flow on one of the grids using two different time steps ($\Delta t^+ = 0.001$ and 0.0005).

The effects of spatial and temporal resolution on the pitching moment coefficient history are shown in Fig. 1. This figure shows that reducing Δt^+ by a factor of 2 has essentially no effect on the computed C_m. The pitching moment coefficient histories obtained on the three grids are also in excellent agreement for $t^+ < 2.6$, up to which time the discussion of the computed results will be limited. It should be noted that the pitching moment, on all grids, at $\alpha = 25$ deg is -0.081, which compares well with the experimental value -0.078 reported by Hummel[39] for a 76-deg sweep delta wing. The effects of numerical resolution on the lift and drag coefficient histories (not included) were found to be even smaller than those for C_m.

The influence of grid resolution and time step on the instantaneous vortex burst location (as determined from the stagnation point along the vortex axis) is shown in Fig. 2. (For convenience, the vortex axis is defined as a ray emanating from the wing apex and passing through the point of minimum total pressure on a crossflow plane ahead of vortex breakdown.) Here again, all computations agree reasonably well with each other. Finally, a comparison of the solutions on the two finest grids at $t^+ = 2.3$ is provided in Fig. 3 in terms of the axial velocity on a plane normal to the wing and passing through the center of the vortex. The location and extent of the computed reversed-flow regions are seen to be in good agreement. The discrepancy between the two solutions in maximum axial reverse velocity magnitude along the vortex core was 4.5%. Although a more systematic numerical resolution study was found to be computationally prohibitive, the previous limited assessment suggests the results are of sufficient quality to merit further analysis. This view is reinforced further by the favorable comparison with experimental measurements that is presented later.

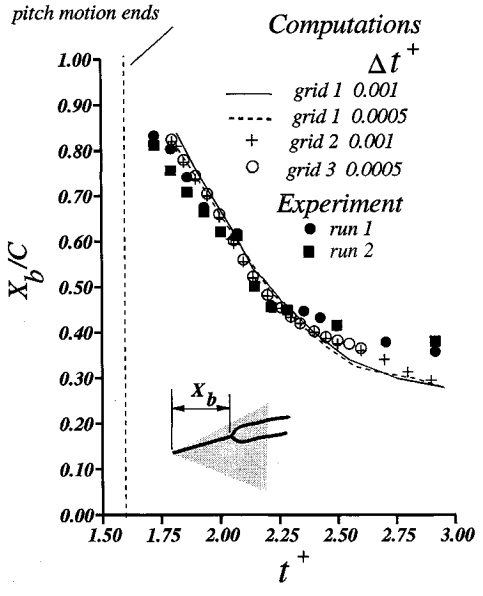

Fig. 2 Computed and experimental vortex breakdown location.

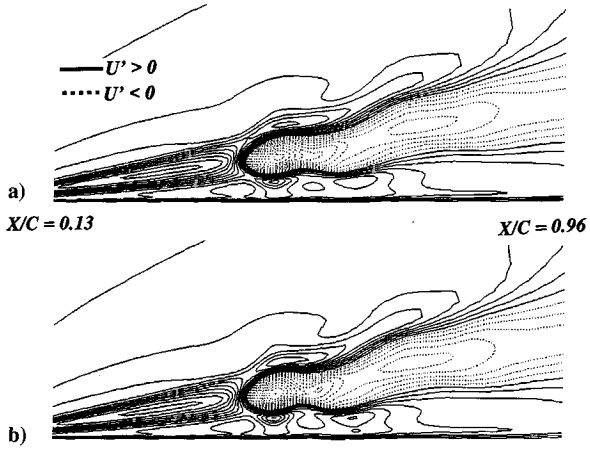

Fig. 3 Effect of grid resolution on axial velocity in a vertical plane through vortex core at $t^+ = 2.3$ (contours of U'/U_∞ from -3.0 to 3.0 with 0.2 increments): a) grid 2 and b) grid 3.

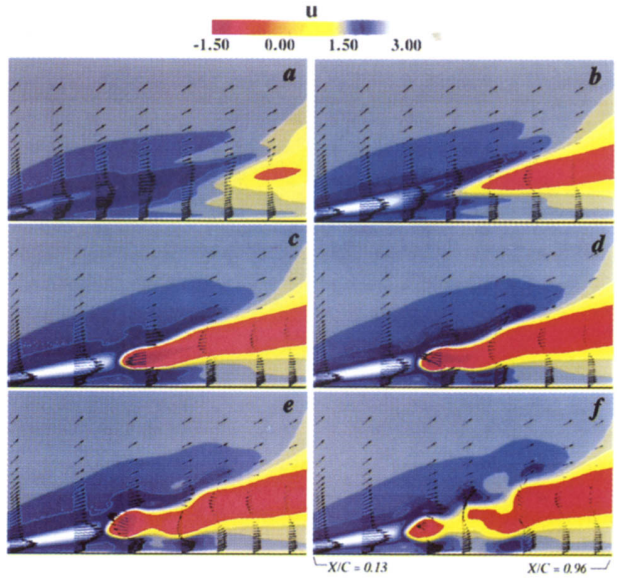

Fig. 4 Axial velocity contours and velocity vectors on plane through vortex core at $t^+ = 1.8$, 2.06, 2.26, 2.3, 2.34, and 2.4.

Evolution of Transient Breakdown

In this section, a description of the initiation and evolution of the breakdown region in the primary leading-edge vortex is provided. In addition to breakdown of the primary vortex, "bursting" or reverse flow in the secondary vortex is also observed. In fact, examination of the computed solution at $t^+ = 0.0$ ($\alpha = 25$ deg) revealed that breakdown of the secondary vortex occurs before the start of the pitching motion. This early breakdown of the secondary vortex, as compared with the main vortex, is consistent with the experimental observations of Lambourne and Bryer.[10] The secondary vortex bursting exerts little influence on the primary flow structure, and therefore details of these secondary features are omitted.

Although the present flow is highly three dimensional, an overall description of the transient breakdown can be obtained from examination of the flow on a longitudinal plane normal to the wing and passing through the center of the vortex core. The angle between this plane and the wing symmetry plane is approximately 10.3 deg. Contours of constant axial velocity and selected velocity vector profiles on this plane, as well as the velocity and pressure along the vortex axis, are given at various instants in Figs. 4–6.

The computed instantaneous position of vortex breakdown, determined from the stagnation point along the vortex axis, is compared in Fig. 2 with results from two separate experimental runs by Lin and Rockwell.[16] The computed and experimental vortex breakdown histories are found to be in good overall agreement. As the burst point moves closer to the apex (say

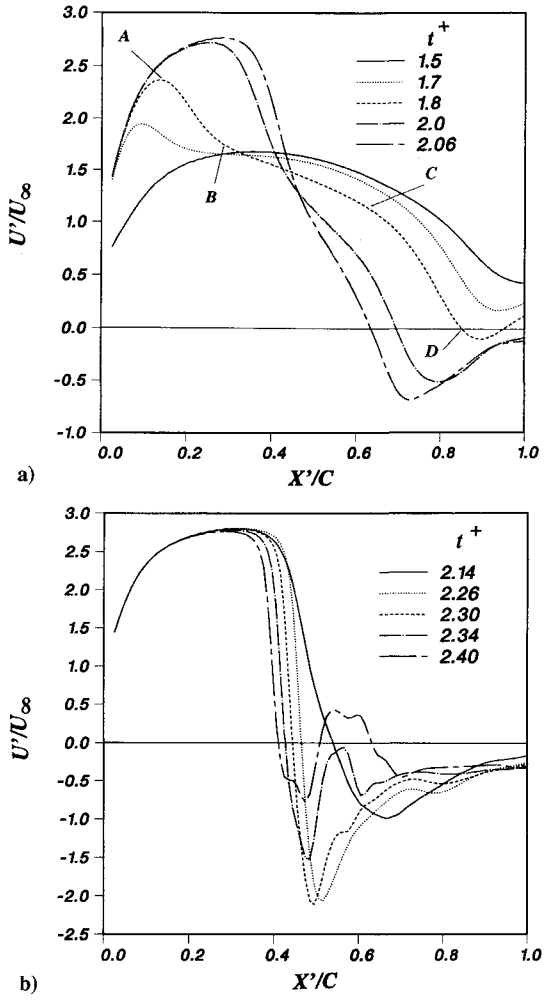

Fig. 5 Evolution of axial velocity component along vortex axis during transient breakdown.

$t^+ > 2.5$), effects of asymmetries in the experiment,[13] present for this high wing sweep, preclude a direct comparison with the fully symmetric calculation. In both the computation and experiment, it is observed that vortex breakdown occurs over the wing only after cessation of the pitching motion ($\alpha = 50$ deg). This shows a significant lag in relation to the stationary case for which breakdown appears[13] near the trailing edge at $\alpha = 31$ deg.

Although a precise explanation of the delay and initial location of vortex bursting is not obvious in this highly transient maneuver, several effects are known to play an important role in this process. For instance, at this high pitch rate and with the pitch axis at the wing trailing edge, the motion induces an apparent longitudinal camber effect.[40] The effective angle of attack at the apex is significantly reduced and increases along the leading edge in the downstream direction (positive camber). The effective local incidences at the apex and trailing edge differ by approximately 17 deg. The elimination of vortex bursting over a stationary cambered delta wing has been clearly shown by Lambourne and Bryer.[10] A significant weakening of the leading-edge vortex occurs as a result of the reduction in effective angle of attack. This can be observed by examining the pressure along the vortex axis (Fig. 6). At $t^+ = 1.5$, despite the high angle of attack of 48 deg, relatively low levels of suction exist in the vortex core near the apex due to the wing pitching motion. In fact, the flow along the vortex core experiences a favorable pressure gradient up to midchord. Shortly afterwards ($t^+ = 1.7$) as the motion ends, and the effective angle of attack increases, high suction levels develop in the vortex core, and an adverse axial pressure gradient appears that promotes breakdown. This severe adverse pressure gradient, imposed abruptly after the end of the pitch maneuver, plays a dominant role in the onset of breakdown. This important pressure gradient effect was also shown experimentally by Sarpkaya[41] for vortex breakdown in a tube.

The pressure gradient along the vortex core becomes more pronounced as breakdown propagates upstream (Fig. 6). As discussed by Hall,[6] the pressure gradient along the axis of a swirling flow is much higher than that prevailing external to the core. This is apparent in Fig. 6, by comparing the pressure along the axis with the corresponding distribution on the wing surface underneath the vortex, at $t^+ = 2.14$. It was also noted in the calculations that the surface pressure does not display significant oscillations under the transient breakdown until approximately $t^+ = 2.26$, when breakdown is already at $X/C = 0.45$. This may have implications on the early detection of breakdown using surface pressure information.

Another effect of importance in transient breakdown is the convective time lags along the vortex core.[10,40] Subsequent to the cessation of the pitching motion, the axial core velocity near the apex increases (Fig. 5a) as the vortex adjusts to the new higher effective incidence. This adjustment of the vortex propagates downstream with a speed on the order of the freestream velocity. As a result, a transient increase in the adverse axial pressure gradient occurs between the regions of higher and lower axial velocities in the core. This effect can be seen between the points denoted as A and B in Fig. 6, at $t^+ = 1.8$.

In the highly transient initial stages of breakdown, following deceleration of the wing, two distinct processes take place along the vortex core. Near the apex, the leading-edge vortex adjusts to a higher effective angle of attack, and this "expansion" (i.e., a region of higher axial velocity and lower pressure) propagates downstream. Simultaneously, stagnation of the axial flow occurs near the trailing edge, and the stagnation region propagates upstream. The axial velocity at $t^+ = 1.8$ (Fig. 5a) clearly shows these effects. From point A to B, a rapid reduction in U' exists associated with the lag in the adjustment of the leading-edge vortex. From point C to D, a high deceleration occurs due to the approaching breakdown region. A plateau in the curve exists between these two regions (point B to C). The extent of this plateau diminishes as the vortex breakdown (moving upstream) and the vortex expansion (moving downstream) collide, roughly at $X/C = 0.5$ and $t^+ = 2.1$.

The overall growth and propagation of the breakdown region is shown in Fig. 4. Also discernable in Figs. 4a–4c is the increase, near the apex, of the axial velocity in the vortex core. At $t^+ = 1.8$ (Fig. 4a), a limited region of axial flow reversal

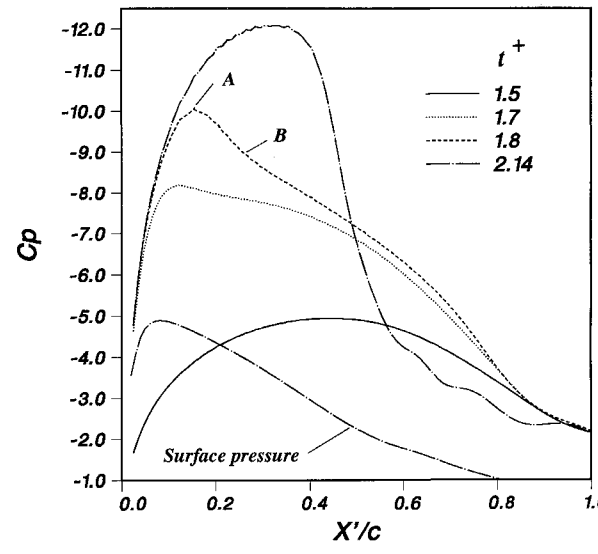

Fig. 6 Evolution of pressure along vortex axis during transient breakdown.

appears ahead of the wing trailing edge and can be observed to extend rapidly in both the upstream and downstream directions. Details of the vortex breakdown downstream of the wing are not considered due to the diminishing grid resolution in this region. As breakdown penetrates upstream (Figs. 4b and 4c), the reversed-flow region grows in radial extent, and its nose becomes blunter due to the increase in radial flow divergence associated with the steepening axial velocity gradient (Fig. 5a). The change in the character of the velocity profiles from a jet type, upstream of breakdown, to a wake type, downstream of breakdown, is also apparent in Fig. 4. During this transient breakdown, very high reversed-flow velocity magnitudes are obtained. At $t^+ = 2.3$ (Fig. 5b), this magnitude exceeds twice the freestream velocity, and consequently, a strong shear layer of azimuthal vorticity surrounds the breakdown region.

In the early stages of the process, the breakdown region appears fairly axisymmetric (Figs. 4a and 4b); however, by $t^+ = 2.26$ (Fig. 4c), some undulations are apparent. These undulations become more pronounced (Figs. 4d and 4e) and lead eventually (Fig. 4f) to the formation of two distinct regions of negative axial velocity. The forward region corresponds to a bubble-type vortex breakdown. It should be noted that, on a crossflow plane between these regions, the axial velocity in the core is everywhere positive. As the breakdown undergoes this dramatic transformation, the magnitude of the reversed-flow velocity diminishes significantly (Fig. 5b), and the breakdown rate of propagation also decreases (Fig. 2).

A comparison of the computed reversed-flow region with the experimental data of Lin and Rockwell[16] is given in Fig. 7 at two instants ($t^+ = 1.9$ and 2.4) during the unsteady breakdown process. The experimental results clearly display the appearance of the bubble structure predicted in the computation. A comparison of computed and experimental axial velocity profiles at a station through the center of the bubble is also shown in Fig. 8. Given the complexity of this highly unsteady flow, the good agreement in Figs. 7 and 8 is encouraging and indicates that the computational approach captures the basic dynamics of the transient breakdown. The emergence of a bubble structure, as the breakdown moves upstream and a stronger jump takes place along the vortex axis (as evidenced, for instance, by the shocklike jump in axial velocity, Fig. 5b), is also consistent with other experimental observations. As shown by Sarpkaya[11] and Faler and Leibovich[12] in their tube experiments, increasing the swirl level sufficiently leads, after initial transients, to the formation of a bubble-type breakdown at a further upstream final location.

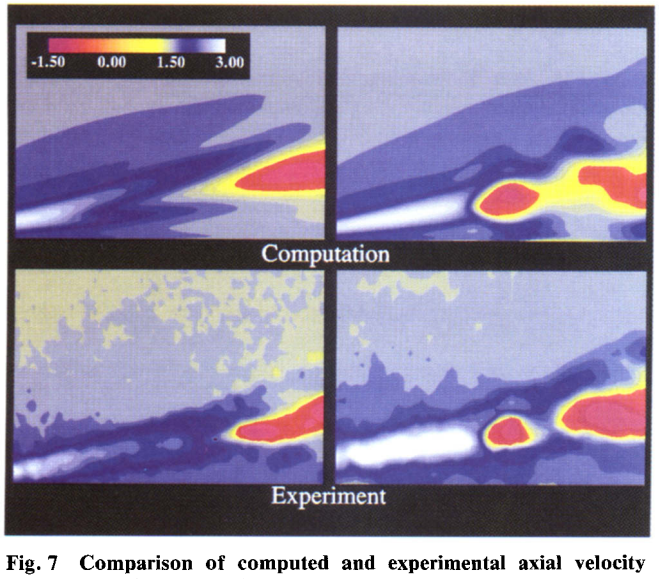

Fig. 7 Comparison of computed and experimental axial velocity contours on plane through vortex core.

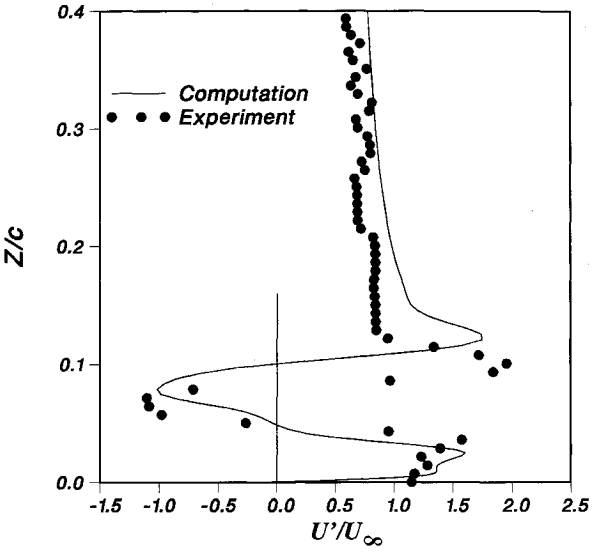

Fig. 8 Comparison of computed and experimental axial velocity profiles through breakdown bubble.

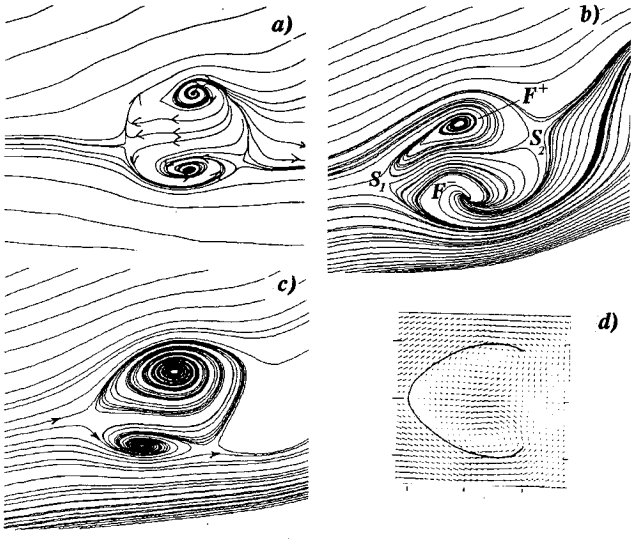

Fig. 9 Sectional streamline patterns on vertical plane through breakdown bubble: a) experiment[16]; b) computed, $t^+ = 2.4$; c) computed, $t^+ = 2.6$; and d) experiment.[18]

Instantaneous Flow Structure

The instantaneous crossflow topology above a pitching delta wing has been investigated experimentally by Magness et al.[13] In the present computational study, the previous experimental findings on the crossflow topology were confirmed and extended, and the results are given in Ref. 42. The evolution of the flow pattern on a longitudinal plane through the vortex core has also been examined, but only the more interesting pattern corresponding to the breakdown bubble of Fig. 4f is shown in Fig. 9. The experimental (Fig. 9a) and computed (Figs. 9b and 9c) patterns (obtained by the projection of the velocity vector on a vertical plane through the center of the bubble) have equivalent topologies of the "single-bubble" type. This pattern is characterized by two saddles (S_1 and S_2), a stable (i.e., spiraling in) focus (F^+), and an unstable (i.e., spiraling out) focus (F^-) and displays no saddle-saddle connections. In the calculations it was found that the three-dimensional bubble (to be described later) rotates about the vortex axis in the same sense as the swirling flow. As a result, the sectional streamline pattern undergoes structural bifurcations.[35,37] This is illustrated in Figs. 9b and 9c, where the foci are observed to switch position relative to the wing, as the bubble rotates. The instantaneous sectional topology seems to

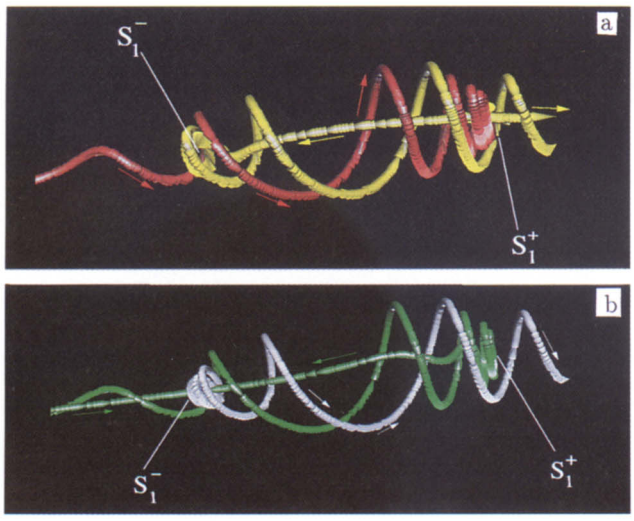

Fig. 10 Three-dimensional critical points and trajectories in vortex breakdown region at $t^+ = 1.8$.

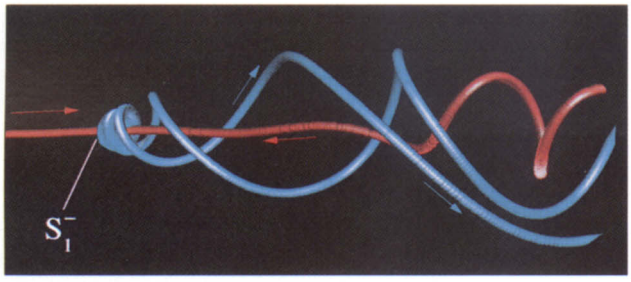

Fig. 11 Three-dimensional critical points and trajectories in vortex breakdown region at $t^+ = 2.06$.

indicate that the bubble is open, thereby allowing upstream flow to go into the bubble, as well as flow from inside the bubble to exit downstream. The streamline pattern obtained for the breakdown bubble above the delta wing (Figs. 9a–9c) is also in qualitative agreement with the recent experiments of Brucker and Althaus[18] for vortex breakdown in a tube, shown in Fig. 9d. Additional comparison of the computed vorticity field within the bubble with the experimental measurements[16,18] is provided in Ref. 43. The computational and experimental instantaneous bubble structure of Fig. 9 seems to be in qualitative agreement with Sarpkaya's original description[11] but differs from the mean axisymmetric topologies described by Faler and Leibovich[44] and Escudier.[9] Furthermore, the present computational results as well as the experimental instantaneous measurements of Refs. 16 and 18 are all characterized by axial reversed-flow velocity magnitudes within the bubble on the order of the freestream velocity (see Fig. 8). This finding contrasts with the very low mean axial velocities inside the bubble reported by Faler and Leibovich[44] and Escudier.[9] However, it should be noted that the relationship between the instantaneous and mean structures of the breakdown bubble requires further investigation.

Although sectional streamlines can provide information on the structure of a complex three-dimensional flow, interpretation based solely on them is incomplete when there is a component of velocity out of the plane under consideration. It should also be noted that the two-dimensional critical points on a planar portrait are not necessarily associated with true critical points of the three-dimensional vector field. To systematically describe the complex instantaneous structure of breakdown above the wing, the three-dimensional velocity vector field is examined, and its topology is characterized in terms of the associated three-dimensional critical points. The three-dimensional free-slip critical points in the breakdown region are shown in Figs. 10–13, along with selected streamlines emanating from or reaching the critical points. For the purpose of reference, the isosurface of zero axial velocity is also included in Fig. 12.

At $t^+ = 1.8$ (Fig. 10), two critical points or stagnation points are observed at the beginning and end of the breakdown region. Point S_1^- is a repelling spiral/saddle or unstable focus/compressing (see Ref. 22), whereas S_1^+ is an attracting spiral/saddle or stable focus/stretching. Only streamlines reaching (red) and leaving (yellow) S_1^+ are shown in Fig. 10a. Similarly, trajectories approaching (green) and leaving (white) S_1^- are included in Fig. 10b. At its onset, the vortex breakdown region, defined by these critical points and associated trajectories, is fairly axisymmetric. As the region of reverse flow grows, point S_1^+ moves downstream of the wing trailing edge and out of the chosen domain of observation, whereas S_1^- proceeds upstream. Later in time ($t^+ = 2.06$, Fig. 11), therefore, only one critical point (S_1^-) is seen and corresponds to the main stagnation point associated with vortex breakdown. Within the reversed-flow region, the streamlines spiral upstream toward S_1^-.

By $t^+ = 2.26$ (Fig. 12), an additional pair of spiral/saddle critical points, denoted as S_2^+ (attracting) and S_2^- (repelling) have emerged. At the instant of the picture, the stagnation points (S_2^+ and S_2^-) are located at approximately the same radial distance from the vortex axis on the isosurface of zero axial velocity and are separated by an azimuthal angle of 85

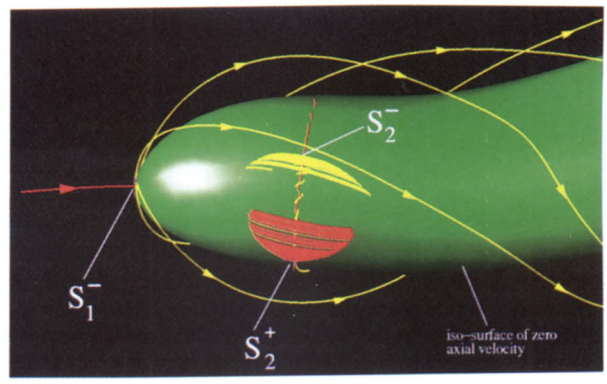

Fig. 12 Three-dimensional critical points and trajectories in vortex breakdown region at $t^+ = 2.26$.

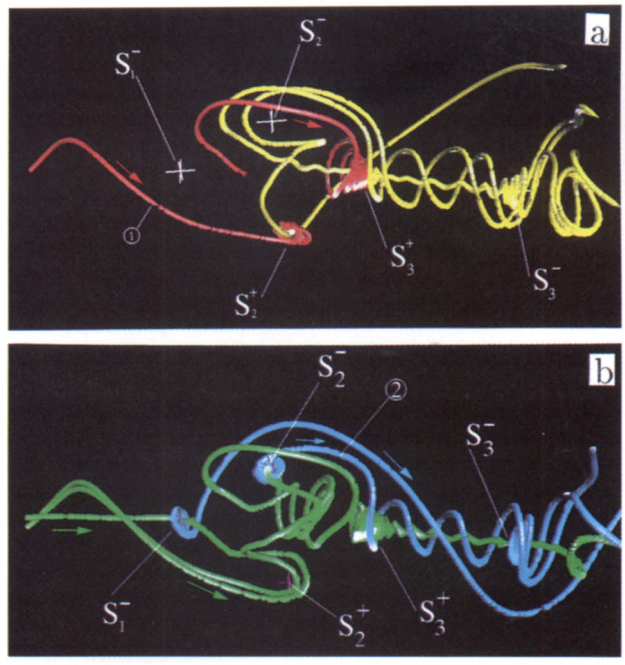

Fig. 13 Three-dimensional critical points and trajectories in vortex breakdown region at $t^+ = 2.4$.

deg. These additional critical points show that multiple stagnation points exist in the breakdown region. A closer look at the way in which S_2^+ and S_2^- are connected is shown in Ref. 45. Observation of the three-dimensional velocity field at various instants in time shows that the critical points (S_2^+ and S_2^-) rotate in the same sense as the swirling flow and move apart from each other in the azimuthal direction. By $t^+ = 2.34$, the approximate azimuthal angle between S_2^+ and S_2^- is 160 deg. Although the reason for the appearance of these critical points is not yet known, they suggest the existence of a growing nonaxisymmetric disturbance. As discussed by Leibovich,[8] as well as shown experimentally by Maxworthy et al.,[46] as axisymmetric waves in a vortex core reach a critical amplitude, instability of the flow to spiral disturbances occurs. The possible relationship between these rotating stagnation points and the experimentally observed coherent oscillations in vortex breakdown also requires further elucidation.

As previously discussed in reference to Fig. 4f, by $t^+ = 2.4$, the breakdown has evolved into two distinct regions of reverse flow. The corresponding three-dimensional topology, given in Fig. 13, indicates the appearance of an additional pair of critical points (S_3^+ and S_3^-). Point S_3^+ is an attracting spiral/saddle associated with the closing of the bubble, whereas point S_3^-, similar to S_1^-, is a repelling spiral/saddle located at the nose of the aft breakdown region. Although only three instantaneous streamlines are shown for each critical point, the complexity of the flow is quite apparent. In Fig. 13a, only the trajectories reaching (red) and leaving (yellow) the attracting spiral/saddles are shown. Similarly, the streamlines approaching (green) and leaving (blue) the repelling critical points (S_1^-, S_2^-, and S_3^-) are included in Fig. 13b. The spiraling trajectory reaching S_2^+ (denoted as 1 in Fig. 13a) goes into the bubble and confirms that the bubble structure is open. Similarly, the trajectory emanating from S_2^- (denoted as 2 in Fig. 13b) goes out of the bubble and spirals along the vortex axis downstream of the bubble. It should also be noted that S_2^+ and S_2^- are approximately 170 deg apart in azimuth. The previous bubble characteristics correlate with the experiments first reported by Sarpkaya[11] and later by Faler and Leibovich,[12] who observed open breakdown bubbles that are filled and emptied at diametrically opposed rotating points.

The relation between the present instantaneous (streamline) structure of breakdown and the available experimental flow visualizations (streaklines) is by no means clear. The complexity revealed by the instantaneous velocity field indicates, however, that the interpretation of the flow structure based solely on standard visualizations is not fully satisfactory. The generation of a streakline representation of the computed transient breakdown for the purpose of comparison was found to be computationally unfeasible. Since the core of the vortex is a region of low total pressure, an alternative representation of breakdown was sought using this scalar quantity. Figure 14a shows an isosurface of constant total pressure at $t^+ = 2.4$. One can clearly observe the vortex core upstream of stagnation, its swelling and bubble formation, as well as a "spiral tail" that winds in a sense opposite to that of the upstream swirl (indicated by the yellow streamline). The computed structure is quite similar to the experimental flow visualization of "axisymmetric" breakdown in a tube obtained by Faler and Leibovich,[12] which is reproduced for convenience in Fig. 14b. This resemblance indicates that vortex bursting over a delta wing at high angle of attack is more closely related to vortex breakdown in a tube than previously shown.

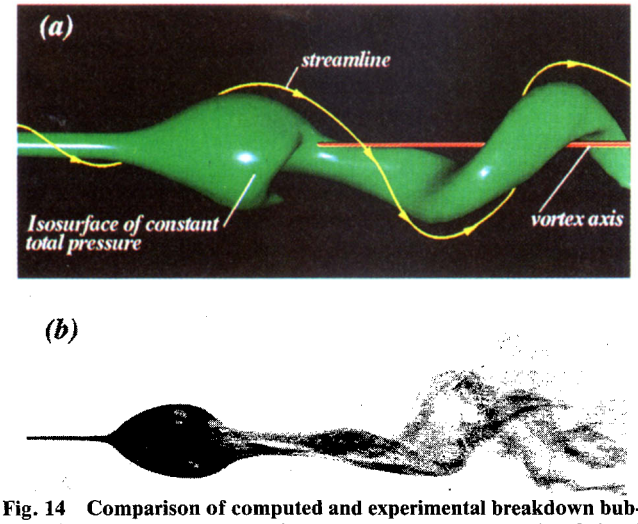

Fig. 14 Comparison of computed and experimental breakdown bubbles: a) computed isosurface of constant total pressure at $t^+ = 2.4$ and b) experimental[12] flow visualization of "axisymmetric" breakdown in a tube.

Concluding Remarks

Computational results have been presented that describe the initiation and evolution of transient vortex breakdown above a delta wing subject to a pitch-and-hold maneuver. The assessment of the effects of numerical resolution and the favorable comparison with available experimental data suggest that the computational approach captures the basic dynamics of this transient breakdown.

The angular delay and onset of breakdown are strongly linked to the pressure gradient prevailing along the vortex axis. This pressure gradient, which depends on the wing angle of attack and pitching motion, plays a dominant role in the initiation of vortex breakdown.

A description of the three-dimensional instantaneous structure of vortex breakdown is provided for the first time using critical-point theory. The region of reverse flow in the vortex core is associated with the appearance of pairs of opposite three-dimensional spiral/saddle critical points. During its early stages, the vortex breakdown is fairly axisymmetric. However, as it proceeds upstream, and a stronger jump takes place along the axis, asymmetric effects become increasingly important and lead eventually to the formation of a breakdown bubble. This bubble structure is open and contains within itself a pair of stagnation points that are diametrically opposed and that rotate in the same sense as the base flow. In accord with recent experimental measurements, the computed results indicate reversed-flow velocity magnitudes within the bubble on the order of the freestream value.

A representation of the breakdown bubble using an isosurface of constant total pressure shows a great deal of resemblance to experimental flow visualizations of axisymmetric vortex breakdown in a tube. Further investigation of the relation between the different representations of the breakdown region (i.e., instantaneous flow structure, streakline visualizations, and mean-flow measurements) should be pursued.

Acknowledgments

I would like to thank D. Rockwell, J.-C. Lin, and C. Magness for providing the experimental data and for their kind assistance in its interpretation. Helpful conversations with R. Gordnier are gratefully acknowledged. Computational resources for this study were provided by the Numerical Aerodynamic Simulation Program (NAS) and by the Air Force Phillips Laboratory, Kirtland Air Force Base, New Mexico.

References

[1]Ashley, H., Katz, J., Jarrah, M.-A., and Vaneck, T., "Unsteady Aerodynamic Loading of Delta Wings for Low and High Angles of Attack," *International Symposium on Nonsteady Fluid Dynamics,* edited by J. Miller and D. Telionis, ASME Fluids Engineering Division, Vol. 92, 1990, pp. 61–78.

[2]Magness, C., Robinson, O., and Rockwell, D., "Control of Leading-Edge Vortices on a Delta Wing," AIAA Paper 89-0999, March 1989.

[3]Jarrah, M.-A., "Low-Speed Wind-Tunnel Investigation of Flow About Delta Wings, Oscillating in Pitch to Very High Angle of

Attack," AIAA Paper 89-0295, Jan. 1989.

[4]Reynolds, G., and Abtahi, A., "Instabilities in Leading-Edge Vortex Development," AIAA Paper 87-2424, Aug. 1987.

[5]Bragg, M. B., and Soltani, M. R., "Measured Forces and Moments on a Delta Wing During Pitch-Up," *Journal of Aircraft,* Vol. 27, No. 3, 1990, pp. 211–217.

[6]Hall, M. G., "Vortex Breakdown," *Annual Review of Fluid Mechanics,* Vol. 4, 1972, pp. 195–218.

[7]Leibovich, S., "The Structure of Vortex Breakdown," *Annual Review of Fluid Mechanics,* Vol. 10, 1978, pp. 221–246.

[8]Leibovich, S., "Vortex Stability and Breakdown: Survey and Extension," *AIAA Journal,* Vol. 22, No. 9, 1984, pp. 1192–1206.

[9]Escudier, M., "Vortex Breakdown: Observations and Explanations," *Progress in Aerospace Sciences,* Vol. 25, 1988, pp. 189–229.

[10]Lambourne, N. C., and Bryer, D. W., "The Bursting of Leading-Edge Vortices—Some Observations and Discussion of the Phenomenon," Aerodynamics Division, NPL, A.R.C., Great Britain, Reports and Memoranda 3282, April 1961.

[11]Sarpkaya, T., "On Stationary and Travelling Vortex Breakdowns," *Journal of Fluid Mechanics,* Vol. 45, Pt. 3, 1971, pp. 545–559.

[12]Faler, J., and Leibovich, S., "Disrupted States of Vortex Flow and Vortex Breakdown," *Physics of Fluids,* Vol. 20, No. 9, 1977, pp. 1385–1400.

[13]Magness, C., Robinson, O., and Rockwell, D., "Instantaneous Topology of the Unsteady Leading-Edge Vortex at High Angle of Attack," *AIAA Journal,* Vol. 31, No. 8, 1993, pp. 1384–1391.

[14]Rediniotis, O., Klute, S., Hoang, N., and Telionis, D., "Pitching-Up Motions of Delta Wings," AIAA Paper 92-0278, Jan. 1992.

[15]Gursul, I., and Ho, C.-M., "Vortex Breakdown Over Delta Wings in Unsteady Free Stream," AIAA Paper 93-0555, Jan. 1993.

[16]Lin, J.-C., and Rockwell, D., "Transient Structure of Vortex Breakdown on a Delta Wing at High Angle of Attack," *AIAA Journal* (to be published).

[17]Towfighi, J., and Rockwell, D., "Instantaneous Structure of Vortex Breakdown on a Delta Wing via Particle Image Velocimetry," *AIAA Journal,* Vol. 31, No. 6, 1993, pp. 1160–1162.

[18]Brucker, C., and Althaus, W., "Study of Vortex Breakdown by Particle Tracking Velocimetry (PTV). Part 1: Bubble-Type Vortex Breakdown," *Experiments in Fluids,* Vol. 13, 1992, pp. 339–349.

[19]Ekaterinaris, J. A., and Schiff, L. B., "Vortical Flows over Delta Wings and Numerical Prediction of Vortex Breakdown," AIAA Paper 90-0102, Jan. 1990.

[20]Spall, R., Gatski, T., and Ash, R., "The Structure and Dynamics of Bubble-Type Vortex Breakdown," *Proceedings of the Royal Society of London, Series A: Mathematical and Physical Sciences,* Vol. 429, 1990, pp. 613–637.

[21]Krause, E., "The Solution to the Problem of Vortex Breakdown," *Lecture Notes in Physics,* edited by K. W. Morton, Vol. 371, 1990, pp. 35–50.

[22]Chong, M. S., Perry, A. E., and Cantwell, B. J., "A General Classification of Three-Dimensional Flow Fields," *Physics of Fluids A,* Vol. 2, No. 5, 1990, pp. 765–777.

[23]Pulliam, T. H., and Steger, J. L., "Implicit Finite-Difference Simulation of Three-Dimensional Compressible Flow," *AIAA Journal,* Vol. 18, No. 2, 1980, pp. 159–167.

[24]Beam, R. M., and Warming, R. F., "An Implicit Factored Scheme for the Compressible Navier-Stokes Equations," *AIAA Journal,* Vol. 16, No. 4, 1978, pp. 393–402.

[25]Pulliam, T., "Artificial Dissipation Models for the Euler Equations," *AIAA Journal,* Vol. 24, No. 12, 1986, pp. 1931–1940.

[26]Rai, M., and Chakravarthy, S., "An Implicit Form of the Osher Upwind Scheme," *AIAA Journal,* Vol. 24, No. 5, 1986, pp. 735–743.

[27]Gordnier, R. E., and Visbal M. R., "Unsteady Vortex Structure over a Delta Wing," *Journal of Aircraft,* Vol. 31, No. 1, 1994, pp. 243–248.

[28]Visbal, M. R., "Numerical Investigation of Laminar Juncture Flows," AIAA Paper 89-1873, June 1989.

[29]Webster, W. P., and Shang, J. S., "Comparison Between Thin-Layer and Full Navier-Stokes Simulations over a Supersonic Delta Wing," *AIAA Journal,* Vol. 29, No. 9, 1991, pp. 1363–1369.

[30]Visbal, M., "Structure of Laminar Juncture Flows," *AIAA Journal,* Vol. 29, No. 8, 1991, pp. 1273–1282.

[31]Stanek, M., and Visbal, M., "Investigation of Vortex Development on a Pitching Slender Body of Revolution," *Journal of Aircraft,* Vol. 30, No. 5, 1993, pp. 711–718.

[32]Gordnier, R., and Visbal, M., "Numerical Simulation of Delta-Wing Roll," AIAA Paper 93-0554, Jan. 1993.

[33]Whitfield, D., "Three-Dimensional Unsteady Euler Equation Solutions Using a Flux Vector Splitting," Short Course on Numerical Grid Generation, Mississippi State Univ., Mississippi State, MS, June 1984.

[34]Tobak, M., and Peake, D., "Topology of 3D Separated Flows," *Annual Review of Fluid Mechanics,* Vol. 14, 1982, pp. 61–85.

[35]Chapman, G. T., and Yates, L. A., "Topology of Flow Separation on Three-Dimensional Bodies," *Applied Mechanics Reviews,* Vol. 44, No. 7, July 1991, pp. 325–345.

[36]Perry, A., and Chong, M., "A Description of Eddying Motions and Flow Patterns Using Critical-Point Concepts," *Annual Review of Fluid Mechanics,* Vol. 19, 1987, pp. 125–155.

[37]Dallmann, U., "On the Formation of Three-Dimensional Vortex Flow Structures," DFVLR-AVA, DFVLR Rept. IB 221-85 A 13, Gottingen, Germany, Aug. 1985.

[38]Globus, A., Levit, C., and Lasinski, T., "A Tool for Visualizing the Topology of Three-Dimensional Vector Fields," Visualization '91, San Diego, CA, Oct. 1991.

[39]Hummel, D., "On the Vortex Formation over a Slender Wing at Large Angles of Incidence," AGARD CP-247, Oct. 1978, pp. 15-1–15-7.

[40]Ericsson, L. E., and Reding, J. P., "Fluid Dynamics of Unsteady Separated Flow. Part II. Lifting Surfaces," *Progress in Aerospace Sciences,* Vol. 24, 1987, pp. 249–356.

[41]Sarpkaya, T., "Effect of Adverse Pressure Gradient on Vortex Breakdown," *AIAA Journal,* Vol. 12, No. 5, 1974, pp. 602–607.

[42]Visbal, M. R., and Gordnier, R. E., "On the Crossflow Topology of Vortical Flows," *AIAA Journal,* Vol. 32, No. 5, 1994, pp. 1085–1087.

[43]Visbal, M. R., "Computational Study of Vortex Breakdown on a Pitching Delta Wing," AIAA Paper 93-2974, July 1993.

[44]Faler, J., and Leibovich, S., "An Experimental Map of the Internal Structure of a Vortex Breakdown," *Journal of Fluid Mechanics,* Vol. 86, Pt. 2, 1978, pp. 313–335.

[45]Visbal, M. R., "Structure of Vortex Breakdown on a Pitching Delta Wing," AIAA Paper 93-0434, Jan. 1993.

[46]Maxworthy, T., Hopfinger, E. J., and Redekopp, L. G., "Wave Motions on Vortex Cores," *Journal of Fluid Mechanics,* Vol. 151, 1985, pp. 141–165.